

Estimation of Functional Connectivity that Causes Burst-like Population Activities

Masaki Nomura^{1,2*}, Daisuke Ito³, Hiroki Tamate³, Kazutoshi Gohara³ and Toshio Aoyagi^{1,2}

¹CREST, JST, Kawaguchi, Saitama, Japan

²Kyoto University, Yoshida-honmachi, Sakyo-ku, Kyoto, Japan

³Hokkaido University, Kita-ku, Sapporo, Japan

*E-mail address: nomura@acs.i.kyoto-u.ac.jp

(Received November 30, 2008; Accepted February 3, 2009)

Rat cortical neurons were cultured, and the multi-dimensional activities from the culture were recorded using 8×8 multi-electrode arrays. As the neurons grew, they built rich synaptic connections, and burst-like population activities were observed in the culture. Using the data during burst-like population activities, the functional connectivity between electrodes was estimated by a dynamic Bayesian analysis. A connection matrix and intrinsic firing rates were obtained from estimation. Then, the binary neuronal network model was simulated with the estimated connection matrix and intrinsic firing rates. The model was found to capture the burst-like population activities. Furthermore, the effect of excitation and inhibition balance on burst-like population activities was explored.

Key words: Network Bursting, Functional Connectivity, Hierarchical Dynamic Bayesian Network, MCMC

1. Introduction

It is known that coordinated burst-like activities emerge in the early developing stage, although their mechanisms and roles remain unknown (Khazipov *et al.*, 2004). It is also known that the firing rates of cultured neurons increase as they grow, and begin to discharge synchronously after a specific stage of growth (Kamioka *et al.*, 1996). Many factors probably underlie the emergence of burst-like activities. Therefore it would seem plausible that it would arise as a result of the formation of a neuronal network. Several authors have studied the functional connectivity of cultured networks (Rigat *et al.*, 2006; Bettencourt *et al.*, 2007). However, under conventional culture conditions, the cell density is so high that visualizing connections between neurons becomes problematic. To overcome this difficulty, we have attempted to culture neurons at very low density. We found recently that neurons cultured even at low density could live for several months and form putative complicated neuronal networks (Ito *et al.*, 2008). Moreover, they showed similar firing rate development and burst-like population activities to neurons cultured in the ordinal density conditions (Ito *et al.*, 2008). Using the multi-dimensional activities, we estimated the functional connectivity of neurons cultured at low density based on the probabilistic model proposed by Rigat *et al.* (2006). With the obtained model, we were able to reproduce burst-like population activities, and with weaker inhibition, hyper-burst activities arose.

2. Cell Culture at Low Density and Immunocytochemistry

We cultured dissociated neurons derived from rat cortex (17-day old embryos, SUMITOMO BAKELITE Co., LTD., Tokyo, Japan) on poly(ethyleneimine)-coated multi-

electrode arrays (MEAs), where the distance between adjacent electrodes is $150 \mu\text{m}$ (see Figs. 1(a) and (b)). The dissociated cells were plated on 64 electrode planar MEAs (Alpha MED Science Co., Osaka, Japan) at a density of 500 cells/ mm^2 (Fig. 1(b)). The cells were maintained at 37 Celsius in a humidified atmosphere of 5% CO_2 and cultured for 35 days in Neuron Culture Medium (SUMITOMO BAKELITE Co., Tokyo, Japan). Half of the culture medium was changed once a week. Spontaneous electrical activity was recorded at 35 days *in vitro* (DIV) for 5 minutes (Fig. 1(c)) with a sampling rate of 20 kHz using MED 64 system (Alpha MED Sciences). Spikes were detected at each electrode by thresholding based on noise level. Even in the low density culture condition, the network seemed to form very complicated structures, and showed synchronous burst activities (Ito *et al.*, 2008) (Figs. 2 and 4). This result suggests that the intrinsic features of the neurons are retained in low-density culture.

To clarify the morphological properties of the network in detail, after recording neuronal activities, immunocytochemistry of the neurons was performed. Cells were fixed with 4% formaldehyde in PBS for 10 min and permeabilized with 0.5% TritonX-100 in PBS for 10 min. Non-specific sites were blocked with 10% Normal Goat Serum (NGS) in PBS for 1 h. Cells were incubated overnight at 4 Celsius with primary antibodies: mouse anti-MAP2 (1:200, Sigma-Aldrich, Japan), rabbit anti-Neurofilament 200 (NF200) (1:200, Sigma-Aldrich, Japan). After washing with PBS, cells were incubated for 1 hour with secondary antibodies: 0.4% Alexa fluor 488 goat anti-mouse IgG (Molecular Probes, Japan), 0.4% Alexa fluor 546 goat anti-rabbit IgG (Molecular Probes, Japan). After washing with PBS again, the nuclei of cells were stained for 10 min

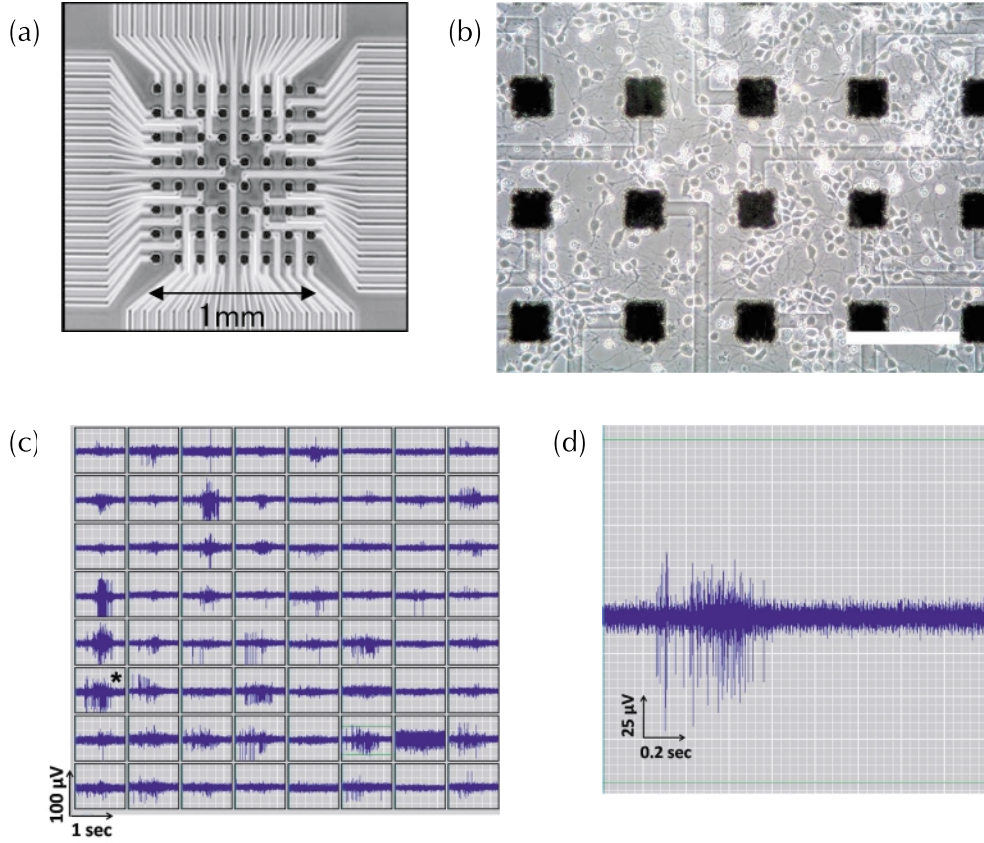


Fig. 1. (a) MEAs substrate. (b) Neurons cultured on MEAs. The scale bar indicates $150 \mu\text{m}$. The black squares are electrodes. (c) Extracellular potential traces of neurons. The activities are detected on electrode. (d) An enlarged view of the activity at one electrode marked with an asterisk in (c).

with $2 \mu\text{g/mL}$ Hoechst 33342 (Molecular Probes, Japan). The network was visualized by staining the cells with antibodies to MAP2 and to NF200 to identify neuronal cell bodies, dendrites and axons, respectively. Fluorescence images were captured using Olympus IX-71 microscope equipped with epi-fluorescence devices. The network structure was visible by low-density cultivation (Fig. 3).

3. Probabilistic Model

Since we are interested in the structure of the network, we tried to estimate the structure of the network from the multi-dimensional spiking activities using a probabilistic model proposed by Rigat *et al.* (2006). Because there are only a small number of neurons on a single electrode, and we are considering only the rough architecture of the cultured network, we confined the estimation of the functional connectivity to between electrodes and not neurons. In the following, we briefly introduce the analytic method.

We assume that the firing probability of the electrode i at a given time t follows the Bernoulli distribution given below:

$$\pi_{it} = \begin{cases} (1 + e^{-\theta_i})^{-1} & t = 1 \\ (1 + e^{-\theta_i - h_i(t)})^{-1} & t > 1 \end{cases} \quad (1)$$

$$h_i(t) = \sum_{j=1}^N \beta_{ij} \frac{\sum_{w=\tau_{it}^{t-1}} Y_{jw}}{t - \tau_{it}}. \quad (2)$$

Here, Y is $N \times T$ (N is the number of electrodes, T

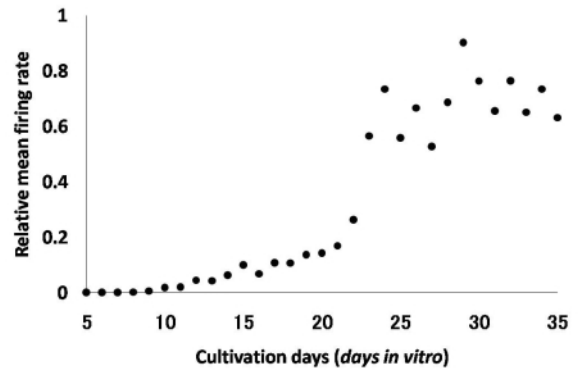


Fig. 2. Relative mean firing rate of growing neurons. We recorded activities for 5 minutes every day and calculated the mean firing rates. After 20 DIV, spontaneous burst-like population activities occurred.

is the time length) multi-dimensional spike data, θ_i is the parameter related to the intrinsic firing rate of the electrode i , β_{ij} is the strength of connection from the electrodes j to i , and τ_{it} represents the latest spike time of the electrode i prior to the time t . If we assume that the activities of the electrodes are independent and spiking is a renewal process, the likelihood related to the data Y is given by Eq. (3):

$$P(Y | \theta, \beta) = \prod_{i=1}^N \frac{e^{Y_{i1}\theta_i}}{1 + e^{\theta_i}} \prod_{t=2}^T \prod_{i=1}^N \frac{e^{Y_{it}(\theta_i + h_i(t))}}{1 + e^{\theta_i + h_i(t)}}. \quad (3)$$

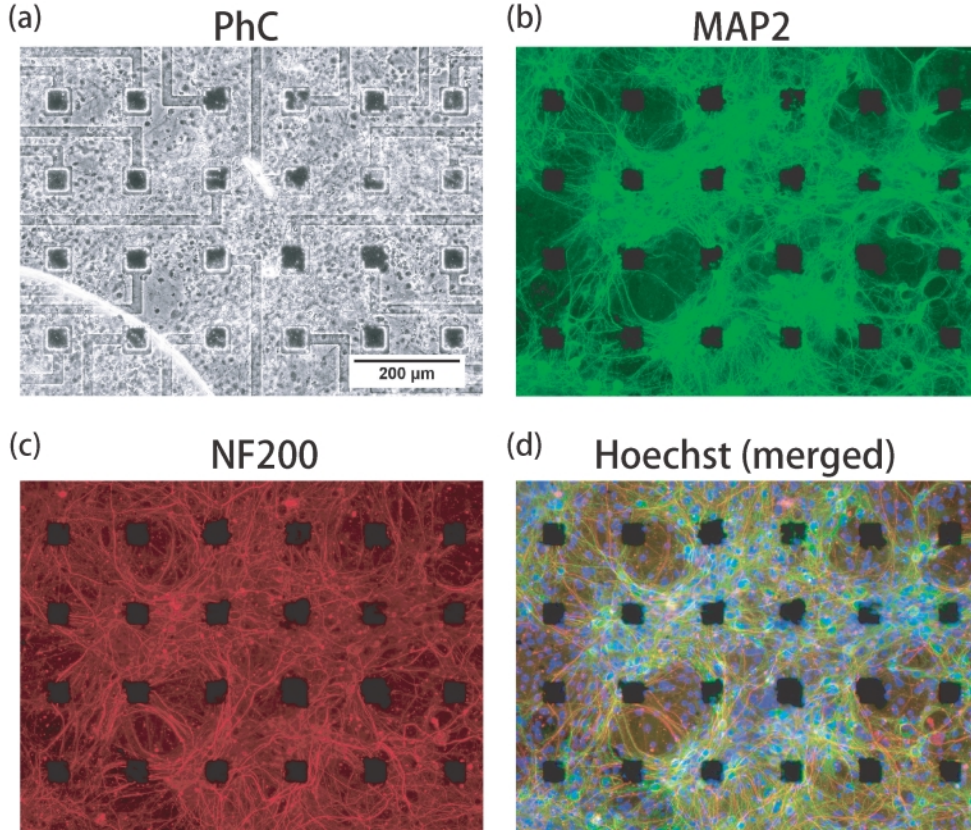


Fig. 3. Fluorescence micrographs of neuronal network on MEAs. (a) Phase contrast micrograph. (b) Somata and dendrites of neurons were stained with antibody to MAP2. (c) Axons of neurons were stained with antibody to NF200. (d) Merged micrograph of MAP2, NF200 and Hoechst 33342.

To estimate the parameters θ and β , we assume the following prior distributions:

$$\alpha_0, \alpha \stackrel{ind.}{\sim} N(0, s_\alpha^2) \quad (4)$$

$$v_{ij} | \alpha_0, \alpha, x_{ij} \stackrel{ind.}{\sim} \frac{e^{(\alpha_0 + \alpha x_{ij}) v_{ij}}}{1 + e^{\alpha_0 + \alpha x_{ij}}} \quad (5)$$

$$\sigma^2 \sim IG(a, b) \quad (6)$$

$$\sigma_{ij} = \sigma(v_{ij} + \epsilon(1 - v_{ij})) \quad (7)$$

$$\beta_{ij} | v_{ij}, \sigma, \epsilon \stackrel{ind.}{\sim} N(0, \sigma_{ij}^2) \quad (8)$$

$$\theta \sim N(0, s_\theta^2 I_K). \quad (9)$$

Here, x_{ij} denotes the distance between the electrodes i and j , and s_θ^2 , ϵ , a , b , and s_α^2 are hyper parameters. $IG(\cdot, \cdot)$ and $N(\cdot, \cdot)$ are the Inverse Gamma distribution and Gauss distribution, respectively.

Using the Bayesian formula, we calculate the posterior distribution from the likelihood:

$$f(\alpha | s_\alpha, X, v, \alpha_0) \propto \phi(\alpha | s_\alpha) \prod_{ij} \frac{e^{\alpha x_{ij} v_{ij}}}{1 + e^{\alpha_0 + \alpha x_{ij}}} \quad (10)$$

$$f(\alpha_0 | s_\alpha, X, v, \alpha) \propto \phi(\alpha_0 | s_\alpha) \prod_{ij} \frac{e^{\alpha_0 v_{ij}}}{1 + e^{\alpha_0 + \alpha x_{ij}}} \quad (11)$$

$$P(v_{ij} = 1 | \beta_{ij}, \alpha_0, \alpha, x_{ij}, \sigma, \epsilon) = \frac{\phi(\beta_{ij} | \sigma) e^{\alpha_0 + \alpha x_{ij}}}{\phi(\beta_{ij} | \sigma) e^{\alpha_0 + \alpha x_{ij}} + \phi(\beta_{ij} | \sigma \epsilon)} \quad (12)$$

$$P(\sigma^2 | a^*, b^*) = IG(a^*, b^*) \quad (13)$$

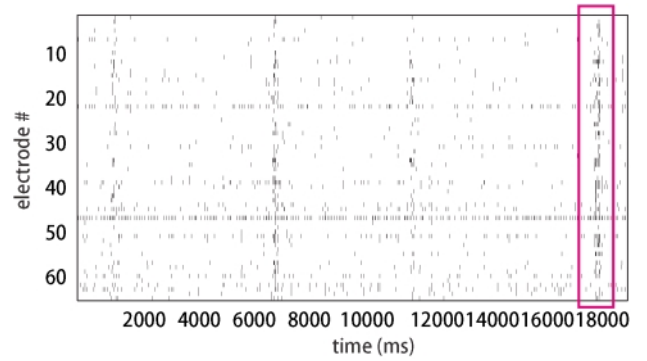


Fig. 4. Burst-like population activities of the network. Using the time-series data enclosed, we estimate the parameters.

$$a^* = a + \frac{K^2}{2} \quad (14)$$

$$b^* = b + \frac{1}{2} \sum_{ij} \frac{\beta_{ij}^2}{v_{ij} + \epsilon^2(1 - v_{ij})} \quad (15)$$

$$f(\beta_{i,:} | Y, v_{i,:}, \beta_{i,-:}, \sigma, \epsilon, \theta_i) \propto \prod_{j=1}^K \phi(\beta_{ij} | \sigma_{ij}) \prod_{t=2}^T \frac{e^{Y_{it} \beta_{ij} \frac{\sum_{w=t_{it}}^{t-1} Y_{jw}}{t-t_{it}}}}{1 + e^{\theta_i + \sum_{k=1}^K \beta_{ik} \frac{\sum_{w=t_{ik}}^{t-1} Y_{kw}}{t-t_{ik}}}} \quad (16)$$

$$f(\theta_i | Y, \beta, \theta_{-i}, s_\theta) \propto \phi(\theta_i | s_\theta) \cdot \prod_{t=1}^T \frac{e^{Y_{it} \theta_i}}{1 + e^{\theta_i + \sum_{j=1}^K \beta_{ij} \frac{\sum_{w=t_{ij}}^{t-1} Y_{jw}}{t-t_{ij}}}} \quad (17)$$

$$\sigma_{ij} = \sigma(v_{ij} + \epsilon(1 - v_{ij})). \quad (18)$$

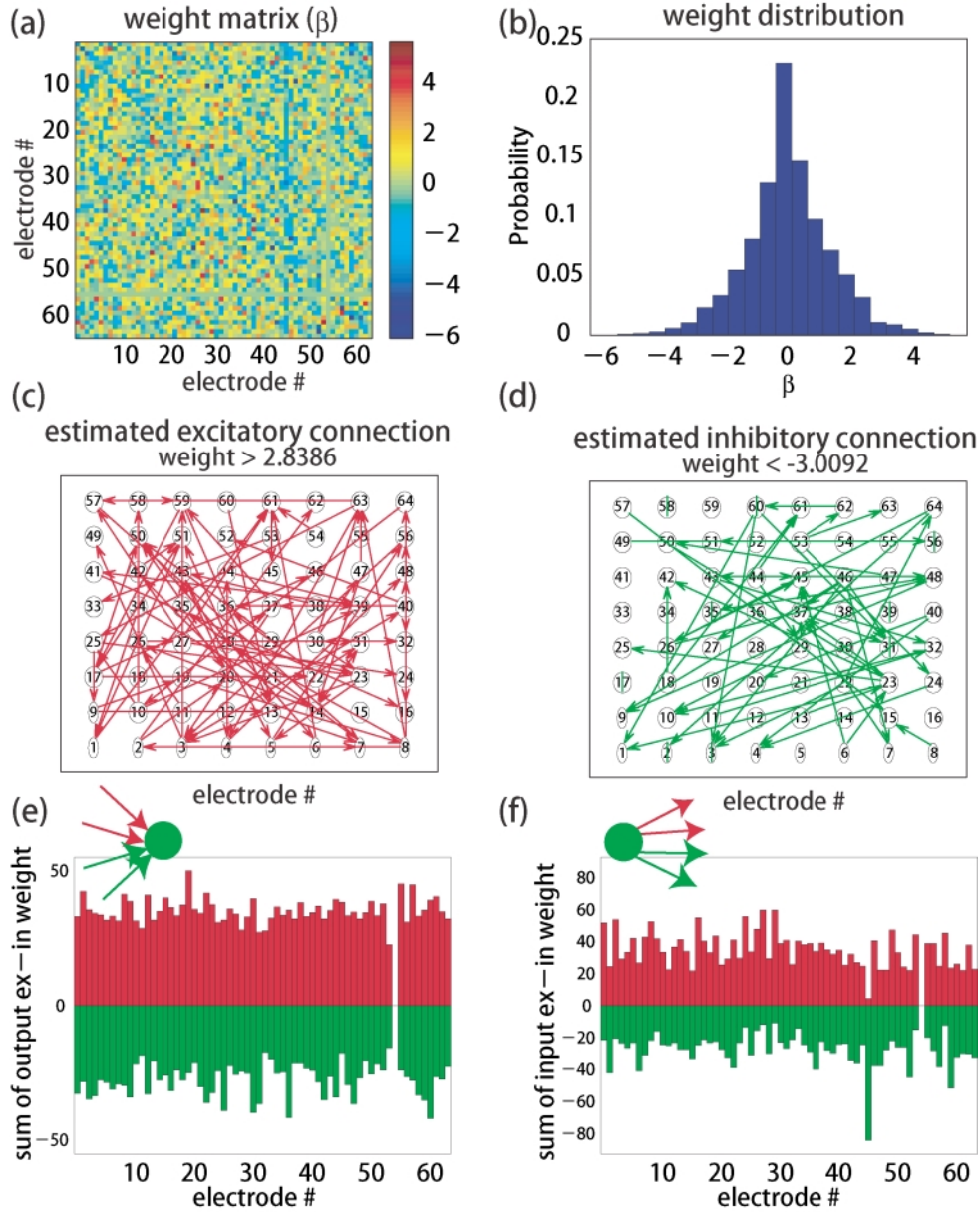


Fig. 5. (a) Estimated values of the parameter $\{\beta_{ij}\}$. (b) The distribution of the parameter β . The estimated network is well balanced in excitation and inhibition. (c) (d) Visualization of excitatory (c) and inhibitory (d) connections that have large coupling weights. (e) (f) Sum of output (e) and input (f) weights of excitatory (red) and inhibitory (green) couplings each. On the 55th electrode, we observed no spikes. Thus, we did not estimate the parameters of this electrode. See also Fig. 6(b).

Here, the function f means an unnormalized probability distribution, and $\phi(x | \sigma)$ means that the variable x is Gaussian distributed, with mean 0 and variance σ^2 .

4. Analytic Results

Using the data from burst-like population activities shown in Fig. 4, we estimated the firing rate θ and the connection strength β . Using the Markov Chain Monte Carlo method, we sampled the values of these parameters with the posterior distributions Eqs. (10)–(17), and adopted the mean values as the parameter value estimates. The results are given in Figs. 5(a) and 6(b). The network with the estimated parameters displays well balanced excitatory and inhibitory couplings (Fig. 5(b)). In Figs. 5(c) and (d), we illustrated the excitatory and inhibitory connections that have

large coupling weights on the alignment of the electrodes. We see that even distant electrodes are connected with large weights. Figures 5(e) and (f) show the sum of output and input weights in each unit, where we see that excitatory and inhibitory inputs are balanced. In contrast, the outputs are set so that at each site either excitation or inhibition is dominant.

Using the estimated parameters, we evolved the network from an initial condition where all the electrodes are silent. At first, the electrodes fired by themselves according to their intrinsic firing rates. Then, they fired synchronously at times (Fig. 6(a)). We see that the characteristics of these burst-like population activities depend on the excitation-inhibition balance. For example, when the strength of the inhibition was reduced by 5%, the frequency

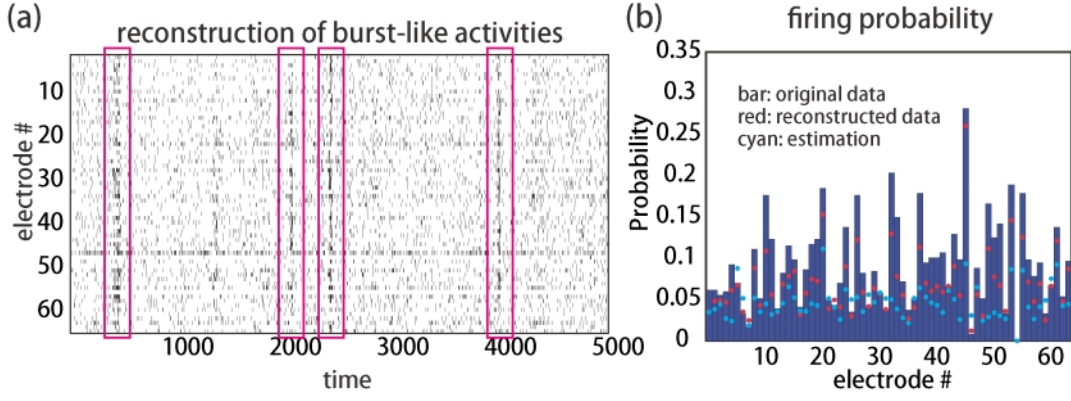


Fig. 6. (a) Using the estimated parameters, we reconstructed burst-like population activities. (b) Comparison of firing rates between the original data, the estimated parameter and the reconstructed data. Here, the estimated value of $\{\theta_i\}$ is transformed into the firing rate by $(1 + \exp(-\theta_i))^{-1}$. The firing rates of the reconstructed data are well matched to those of the original data.

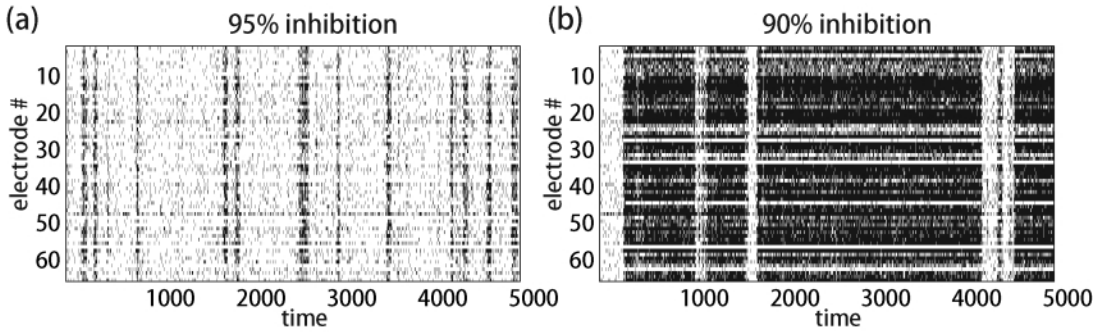


Fig. 7. The simulation results in the cases of reduced inhibitory strength ((a) 95%, (b) 90%). The time length of burst activities elongated in weak inhibition.

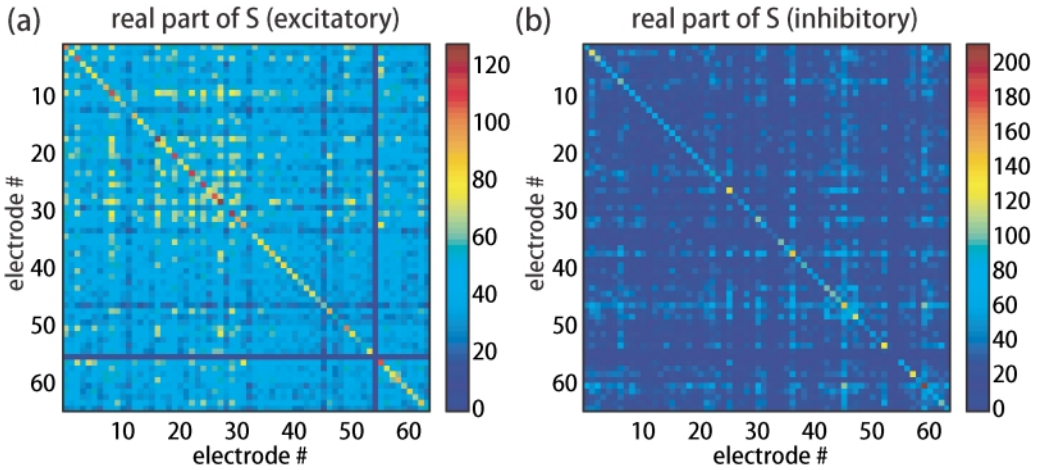


Fig. 8. (a) The real part of matrix S calculated from the excitatory coupling strength β^{ex} . (b) Same as (a) but calculated from β^{in} .

of burst-like population activities increased (Fig. 7(a)). Furthermore, when reduced by 10%, hyper-burst activities occurred (Fig. 7(b)).

In order to visualize the structure of the network, we attempted to find cliques in the network. We analyzed the connection matrix β by using a cluster detecting algorithm proposed by Hoser and Schröder (2007). Since our connection matrix β is asymmetric, conventional spectral cluster-

ing algorithms can not be applied to it. Hoser et al. circumvent this problem by introducing a complex matrix. The procedure of their algorithm is the following:

- 1) Calculate the Hermitian matrix H from the adjacency matrix β by the transformation $H = (\beta + i\beta^T) \exp(-i\pi/4)$, where β^T is the transpose of β .
- 2) Solve the eigenvalue problem of H and build a matrix

R ,

$$R = \begin{pmatrix} \lambda_1^+ x_{11}^+ & \cdots & \lambda_l^+ x_{l1}^+ \\ & \cdots & \\ \lambda_1^+ x_{1N}^+ & \cdots & \lambda_l^+ x_{lN}^+ \end{pmatrix}, \quad (19)$$

where N and l are the number of the electrode and the number of the positive eigenvalues, respectively. The eigenvalues are sorted in descending order, that is, $\lambda_1^+ \geq \lambda_2^+ \geq \cdots \geq \lambda_l^+ > 0$, and $(x_{i1}^+, \dots, x_{iN}^+)^T$ is the eigenvector corresponding to its eigenvalue λ_i^+ .

- 3) Calculate the matrix S by $S = RR^*$, where R^* is the Hermitian matrix of R .
- 4) The real part of S is a similarity matrix, which determines the memberships of cliques between the electrodes.

Note that in this algorithm, the elements of the adjacency matrix β must be positive and all the diagonals must be zero. Therefore, we separated the estimated matrix β into matrices related to the excitatory network β^{ex} and the inhibitory network β^{in} . The elements of the matrix β^{in} were taken as their absolute values. We analyzed the matrices β^{ex} and β^{in} separately, and the real part of the matrix of S is shown in Figs. 8(a) and (b) each. In these figures, we see that there are no clear clusters of electrodes in the excitatory and inhibitory networks, although in the excitatory network, there seem several weak clusters.

5. Conclusion and Discussion

We cultured rat cortical neurons on multi-electrode arrays at low density, and recorded neuronal activities simultaneously. We observed that burst-like population activities occurred after about 20 DIV. Around this time, we stained the neurons to visualize the emergent network, where it was seen that the dendrites and the axonal arbors of the neurons spread widely, forming what seemed to be a complex network.

We estimated the structure of the network between electrodes based on the spiking activities using a probabilistic model. This network reproduced burst-like population activities. We also simulated the network with its inhibition reduced and observed the resultant hyper-burst activities.

The result shows that the burst-like population activities arise from excitation-inhibition balance.

Although the network with parameters inferred from the data reproduced burst-like population activities, many problems are left to be solved. Firstly, recorded activities must be separated into single unit activities. In our analysis, we treated the activities on electrodes and estimated the network between them. Secondly, we introduced no internal dynamics in the units (in our case, electrodes) of the probabilistic model. If the burst-like population activities depend on the cell dynamics, the model fails to capture them, although a feed-back excitatory system could be included by self-excitatory connection. Thus, a more complicated model may be needed for further studies.

In the future, we plan to study the effects of drugs on the neuronal networks, and the behavior of our estimated network should be consistent with what is observed in such an experiment. In addition, we plan to infer changes that occur in the network connectivity through the application of electrical stimulus.

Acknowledgments. The network estimation was done by using the BHNNtoolbox, which was developed by Fabio Rigat and can be obtained from <http://www2.warwick.ac.uk/fac/sci/statistics/staff/academic/rigat/software/bhnn/>

References

- Bettencourt, L. M. A., Stephens, G. J., Ham, M. I. and Gross, G. W. (2007) Functional structure of cortical neuronal networks grown in vitro, *Phys. Rev. E*, **75**, 021915.
- Hoser, B. and Schröder, J. (2007) Automatic determination of clusters, in *Operations Research Proceedings 2006* (eds. Waldmann, K.-H. and Stocker, U. M.), pp. 439–444, Springer, Berlin, Heidelberg.
- Ito, D., Tamate, H., Nomura, M., Aoyagi, T. and Gohara, K. (2008) Immunocytochemistry in low-density culture of neurons on multielectrode arrays is effective for identification of action-potential pathway, *Abstracts of Society for Neuroscience*, Program No. 797.16.
- Kamioka, H., Maeda, E., Jimbo, Y., Robinson, H. P. C. and Kawana, A. (1996) Spontaneous periodic synchronized bursting during formation of mature patterns of connections in cortical cultures, *Neuroscience Letters*, **206**, 109–112.
- Khazipov, R., Sirota, A., Leinekugel, X., Holmes, G. L., Ben-Ari, Y. and Buzsáki, G. (2004) Early motor activity drives spindle bursts in the developing somatosensory cortex, *Nature*, **432**, 758–761.
- Rigat, F., de Gunst, M. and van Pelt, J. (2006) Bayesian modelling and analysis of spatio-temporal neuronal networks, *Bayesian Analysis*, **1**(4), 733–764.